https://doi.org/10.5194/egusphere-2025-5017
Preprint. Discussion started: 16 February 2026

Development and validation of ARMS-gb v2.0: Extending fast radiative transfer modeling capability to all-sky conditions for ground-based microwave radiometer retrievals

Ziyue Huang[1,2], Yi-Ning Shi[2,3], Fuzhong Weng[2,3], Jun Yang[2,3]

[1]Department of Atmospheric and Ocean Sciences, Fudan University, Shanghai, 200438, China
[2]State Key Laboratory of Severe Weather Meteorological Science and Technology, CMA Earth System Modeling and Prediction Centre, China Meteorological Administration, Beijing, 100081, China
[3]State Key Laboratory of Severe Weather Meteorological Science and Technology, Chinese Academy of Meteorological Sciences, China Meteorological Administration, Beijing, 100081, China

Correspondence to: Jun Yang (yangjun@cma.gov.cn)

Abstract. Ground-based microwave radiometers provide continuous, all-weather observations of boundary-layer temperature and humidity, closing a critical near-surface observation gap. The Advanced Radiative Transfer Modeling System – ground-based (ARMS-gb) is a fast radiative transfer model specifically designed to simulate the brightness temperatures these instruments observe. This paper presents ARMS-gb v2.0, which introduces modules to calculate absorption and scattering from hydrometeors, and a multi-scattering solver using the discrete ordinate addition method (ADOM). The model now simulates cloud water, rain, ice, snow, and graupel using optical-property look-up tables computed with Mie theory and the discrete dipole approximation (DDA). Other new aspects are the extension of the existing tangent-linear and adjoint (TL/AD) modules to include hydrometeor processes, enabling all-sky retrieval and variational data assimilation. Validation against field measurements from 14- and 22-channel ground-based microwave radiometers indicates that ARMS-gb v2.0 can effectively simulate brightness temperatures under all-sky conditions, with the mean observed minus simulated brightness temperature across all channels kept within 1 K in cloudy cases. Compared with ARMS-gb v1.0, which neglects cloud effects, the root mean square error (RMSE) under cloudy conditions decreases by 1–2 K in the strong water-vapor channels, most notably at 30 GHz, where the correlation improves from 0.34 to 0.71. In the weak oxygen band, the O-B decreases by 3–4 K, particularly at 51 GHz, where the correlation increases from 0.43 to 0.85. Moreover, the results indicate that the DDA model slightly outperforms the Mie model in characterizing frozen hydrometeors at these channels. However, simulation errors increase significantly during precipitation events, and the RMSE in the water-vapor absorption band can reach 30–40 K, which remains a challenge for assimilation and retrieval in such conditions.

1 Introduction

In recent years, extreme weather events have become more frequent and variable, and the planetary boundary layer (PBL) plays a central role in their formation and evolution. The development of low-altitude aviation increases the demand for reliable

https://doi.org/10.5194/egusphere-2025-5017
Preprint. Discussion started: 16 February 2026

boundary-layer observations, which motivates more efficient and accurate measurement techniques and targeted mechanistic studies. Microwave remote sensing operates in the presence of clouds and precipitation and supports long-term continuous unattended monitoring, which provides clear advantages for all-sky applications. The atmospheric absorption coefficient depends on temperature, pressure, and water-vapor density, so boundary-layer variability directly affects microwave opacity and the observed brightness temperatures. Although satellite-based microwave radiometers provide extensive coverage of the atmosphere, they cannot reliably retrieve PBL temperature and humidity over land because land-surface microwave emissivity is highly variable and introduces significant uncertainty in the measured radiances (Martinet et al., 2020). This limitation causes an observation gap between the surface and the upper troposphere (Council et al., 2009), which is precisely the critical region where energy and water-vapor exchanges occur between the land surface and the free atmosphere (Wu et al., 2024).

Ground-based microwave radiometers (GMRs), operated in an upward-looking configuration, provide continuous retrievals of temperature and humidity profiles under all-sky conditions with high temporal resolution and moderate vertical resolution that is concentrated within the PBL (Cimini et al., 2006; Wei et al., 2024). GMRs can capture rapid boundary-layer variability, and contribute to understanding PBL dynamical processes while helping to bridge the observation gap between the surface and the upper troposphere (De Angelis et al., 2017). Compared with radiosondes, GMRs can offer high-frequency, continuous observations that are not affected by wind advection and therefore show stronger regional representativeness, which enables long-duration all-weather monitoring within the PBL (Madhulatha et al., 2013). Under clear-sky conditions, the atmosphere is nearly transparent and dominated by water-vapor absorption. With cloud and precipitation, the optical thickness increases rapidly, and deep convection can become effectively opaque, and path attenuation typically increases with rain rate and frequency. All-sky microwave observations are therefore both valuable and challenging, motivating the development of a fast, accurate all-sky radiative-transfer operator for GMRs.

Radiative transfer models (RTMs) provide the essential link between atmospheric state variables and observed radiances, and fast RTMs are indispensable for variational assimilation in modern numerical weather prediction (NWP) systems (Hu and Han, 2021; Weng and Liu, 2003; Yang et al., 2020). Early applications were limited to clear-sky oceanic conditions due to the difficulty of simulating cloud and precipitation microphysics, as well as surface emissivity. With subsequent advances, mainstream fast RTMs such as CRTM (Weng et al., 2005), RTTOV (Saunders et al., 1999), and ARMS (Weng et al., 2020; Yang et al., 2020) have been extended to all-sky capabilities, which has enabled the operational assimilation of cloud-affected satellite radiances (Bauer et al., 2010; Geer et al., 2017). Despite being less affected by surface emissivity and capable of providing continuous, high temporal resolution boundary-layer observations, the assimilation of GMRs data has lagged behind satellite applications, owing to the lack of suitable forward models and effective methods for handling water vapor and hydrometeor. High-accuracy monochromatic tools (e.g., MonoRTM; Clough et al., 2005), together with absorption models such as MPM (Rosenkranz, 1998), are widely used as references, but they are computationally too expensive for routine, instrument-level broadband simulations at the temporal resolution required by GMR retrieval and data-assimilation applications. When each broadband channel is approximated by a single monochromatic calculation at the channel centre frequency, systematic brightness-temperature biases of a few kelvin (~2–3 K) have been reported (Yang and Min, 2015). To

https://doi.org/10.5194/egusphere-2025-5017
Preprint. Discussion started: 16 February 2026

our knowledge, only two dedicated fast radiative transfer models for ground-based microwave radiometers are currently available, RTTOV-gb in Europe (Cimini et al., 2019) and ARMS-gb in China (Shi et al., 2025a). RTTOV-gb was a significant development, however, recent studies report substantial biases in water-vapor channels (Cao et al., 2023) and the lack of an operational cloud-scattering option, leaving many cloud-affected GMRs observations unused. ARMS-gb v1.0 is a fast radiative transfer model for GMRs that incorporates a line-by-line trained gaseous absorption scheme and an advanced water-vapor vertical interpolation with tangent-linear and adjoint modules for Jacobian evaluation. Validation against benchmark simulations and real observations demonstrated that the performance of ARMS-gb v1.0 is comparable to or better than RTTOV-gb in humid environments and is useful for observation-minus-background (O-B) monitoring. Despite these advances, ARMS-gb v1.0 remains a clear-sky model, and RTTOV-gb accounts only for absorption by cloud liquid water, precluding direct all-sky assimilation of GMR radiances. Additionally, variational systems rely on a forward-model operator with its associated Jacobians, while the observation-error covariance accounts for radiometric noise, representativeness, and forward-model uncertainties. Therefore, a fast and accurate all-sky RTM with tangent-linear and adjoint capabilities is essential. Here, we describe several new aspects of ARMS-gb v2.0, which incorporates hydrometeors scattering and absorption modules together with a numerically stable multiple-scattering solver, and provides forward, tangent-linear, and adjoint modules under all-sky conditions to support the direct assimilation of GMRs observations.

This paper is organized as follows. Section 2 describes the two main developments in ARMS-gb v2.0: the computation of optical properties of hydrometeors and an solver for multiple scattering. Section 3 explores sensitivity to hydrometeor water content and particle size across the water-vapor and oxygen microwave absorption bands. Section 4 evaluates all-sky simulations with the updated RTM against six months of field measurements from ground-based observations collected in China for a 14-channel and a 22-channel GMR, and examines error characteristics and sources for retrieval and data assimilation. Section 5 concludes with a summary and perspectives.

2 Model development

The primary advancement in ARMS-gb v2.0 is the extension from clear-sky to all-sky applications while retaining the gaseous absorption parameterization, clear-sky solver, and vertical interpolation scheme of v1.0 for continuity. In the microwave regime, we solve a scalar radiative transfer equation for brightness temperatures, and atmospheric attenuation is determined by temperature, pressure, water-vapor density, and rain microphysics, so hydrometeors can significantly perturb the radiance field even when gas absorption is well captured. Figure 1 compares the time series of observed and simulated clear-sky brightness temperatures measured by YKW-1, a 22-channel GMR, at Yan'an Station (36.34° N, 109.27° E). For context, the corresponding liquid and solid hydrometeors profiles from the fifth-generation ECMWF atmospheric reanalysis (ERA5, Hersbach et al., 2020) are also shown. The forward simulations simply consider gaseous absorption and do not include any cloud or precipitation scattering information. The simulations accurately track observations during cloud-free periods, whereas departures grow in water-vapor and weak-oxygen channels when hydrometeors are present, which motivates a consistent

https://doi.org/10.5194/egusphere-2025-5017
Preprint. Discussion started: 16 February 2026

representation of their combined effects. To address this, ARMS-gb was updated with two new modules. The first is a cloud optics module that calculates the bulk scattering properties of cloud particles. These properties are derived by integrating the single-particle attributes of various hydrometeors (cloud water, rain, ice, snow, and graupel) over the particle size distribution, utilizing a precomputed look-up table (LUT). The second is an all-sky radiative transfer solver that accounts for multiple scattering and emission, applies appropriate lower boundary conditions, and enables physically consistent simulations under all-sky conditions.

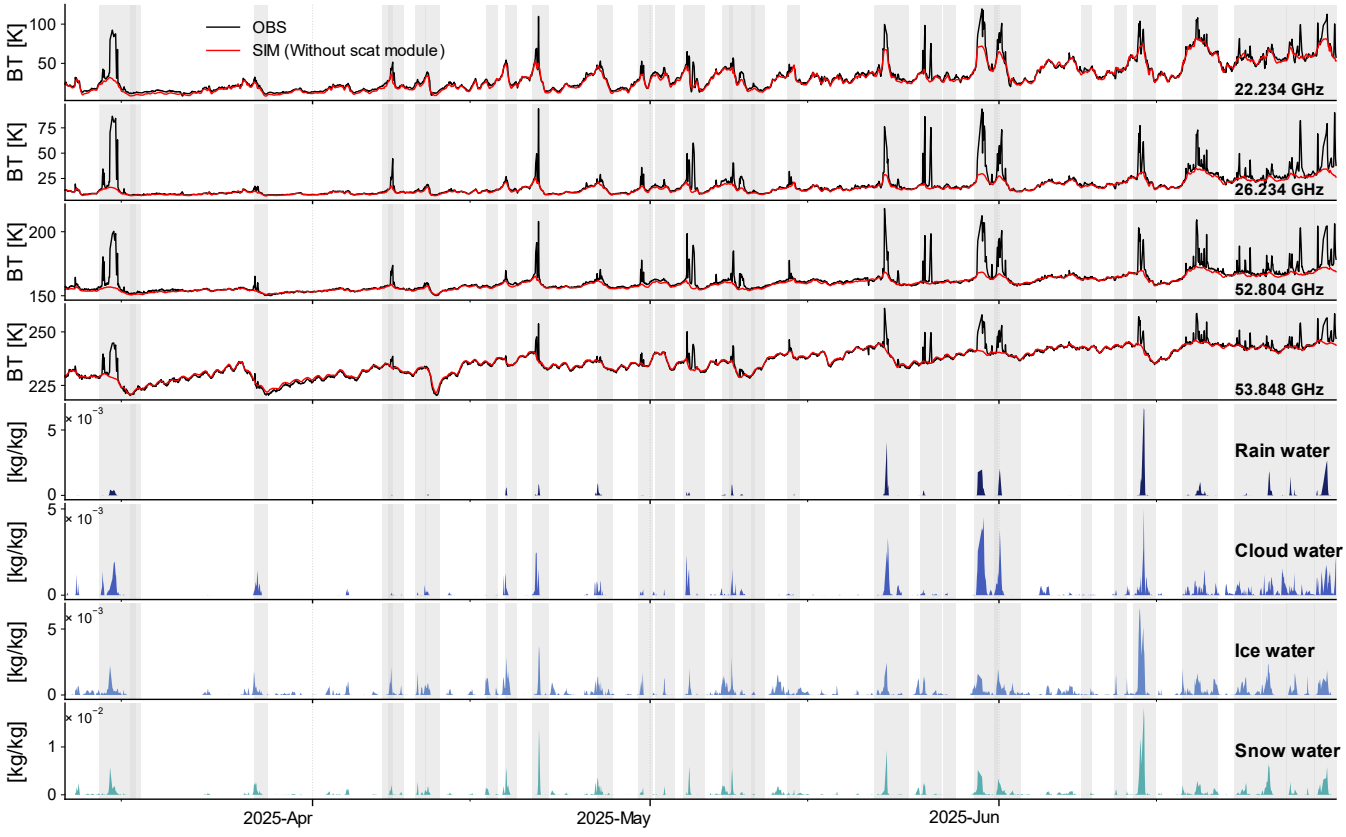

Figure 1: Time series of observed (OBS) and simulated (SIM) brightness temperatures from a ground-based microwave radiometer at Yan'an station from April to June 2025. The simulations were performed using a model without a cloud scattering module. For reference, the corresponding hydrometeor profiles from ERA5 reanalysis for the same period are shown in the bottom panels.

2.1 Cloud particle absorption and scattering module

ARMS-gb v2.0 parameterizes the scattering and absorption properties of cloud and precipitation particles using a pre-computed LUT, following the methods of Huang et al. (2025). The LUT includes five hydrometeor categories: cloud water, rain, ice, snow, and graupel. Single-particle optical properties—extinction coefficient, single-scattering albedo (SSA), and the full phase function—are calculated with Mie theory for liquid droplets and with a rough-surfaced aggregate model, based on the discrete dipole approximation (DDA, Draine and Flatau, 1994), for nonspherical frozen particles. These single scattering properties are

https://doi.org/10.5194/egusphere-2025-5017
Preprint. Discussion started: 16 February 2026

then integrated over a modified gamma size distribution to obtain bulk optical parameters. The LUT is constructed for liquid hydrometeors at temperatures ranging from 275 to 290 K in 5 K intervals and for solid hydrometeors from 243 to 273 K in 10 K intervals. For refractive indices, we adopted the refractive-index data of Ray (1972) for liquid water and the ice model developed by Mätzler (2006), ensuring robustness across the full microwave spectrum and a wide range of temperatures. In addition, for solid hydrometeors (ice, snow, and graupel), their complex refractive indices were further adjusted using the Maxwell–Garnett mixing formulation (Garnett, 1906) to represent the effective dielectric properties of ice–air mixtures. Two types of GMRs are used in this study: the 22-channel YKW-1 and the 14-channel YKW-2, both widely deployed across China. Their respective channel center frequencies are listed in Tables 1 and 2. In this configuration, the channels cover two key absorption regions: the water-vapor band between 22 and 31 GHz and the oxygen absorption band between 51 and 59 GHz. The channel near 22.235 GHz ensures high humidity sensitivity, while the oxygen band provides robust temperature information, making the design well-suited for boundary-layer thermodynamic profiling.

Table 1: Center frequencies of YKW-1

Channel	1	2	3	4	5	6	7	8
Frequency (GHz)	22.234	22.500	23.034	23.834	25.000	26.234	28.000	30.000
Channel	9	10	11	12	13	14	15	16
Frequency (GHz)	51.248	51.760	52.280	52.804	53.336	53.848	54.400	54.940
Channel	17	18	19	20	21	22		
Frequency (GHz)	55.500	56.020	56.660	57.288	57.964	58.800		

Table 2: Center frequencies of YKW-2

Channel	1	2	3	4	5	6	7
Frequency (GHz)	22.240	23.040	23.840	25.440	26.240	27.840	31.040
Channel	8	9	10	11	12	13	14
Frequency (GHz)	51.260	52.280	53.860	54.940	56.660	57.300	58.000

Figure 2 shows that extinction increases monotonically with frequency and effective radius for all hydrometeors between 20 and 60 GHz. Cloud liquid water remains absorption dominated with SSA near zero, so its influence in the 22–31 GHz vapor band and the 51–59 GHz oxygen band is mainly through absorption. Frozen species behave differently. Scattering strengthens rapidly with increasing size and frequency, and once effective radii reach a few hundred micrometers and frequencies exceed about 45–50 GHz, the albedo approaches unity, indicating a scattering-dominated regime that is most evident in the oxygen band. The difference panels use Mie minus DDA and are shown only for frozen species, since cloud-water differences are identically zero when both configurations use Mie. For ice and snow, the differences are small at small radii and low

https://doi.org/10.5194/egusphere-2025-5017
Preprint. Discussion started: 16 February 2026

frequencies and grow to positive values with size and frequency, which means the spherical assumption tends to produce stronger extinction and higher albedo than the nonspherical treatment. Differences for graupel remain comparatively small, consistent with its more compact and near-spherical habit. Band dependence is clear. The 22–31 GHz water-vapor band is only moderately sensitive to frozen-phase scattering, whereas the 51–59 GHz oxygen band is highly sensitive, and the DDA–Mie discrepancies are amplified there. These results imply that nonspherical effects must be represented for ice and snow in the oxygen band and are weaker in the vapor band. In forward modeling and data assimilation, assuming spherical particles tends to overestimate scattering from large frozen hydrometeors in the oxygen band, whereas employing DDA-based optical properties reduces this bias, with the degree of improvement depending on both particle size and frequency.

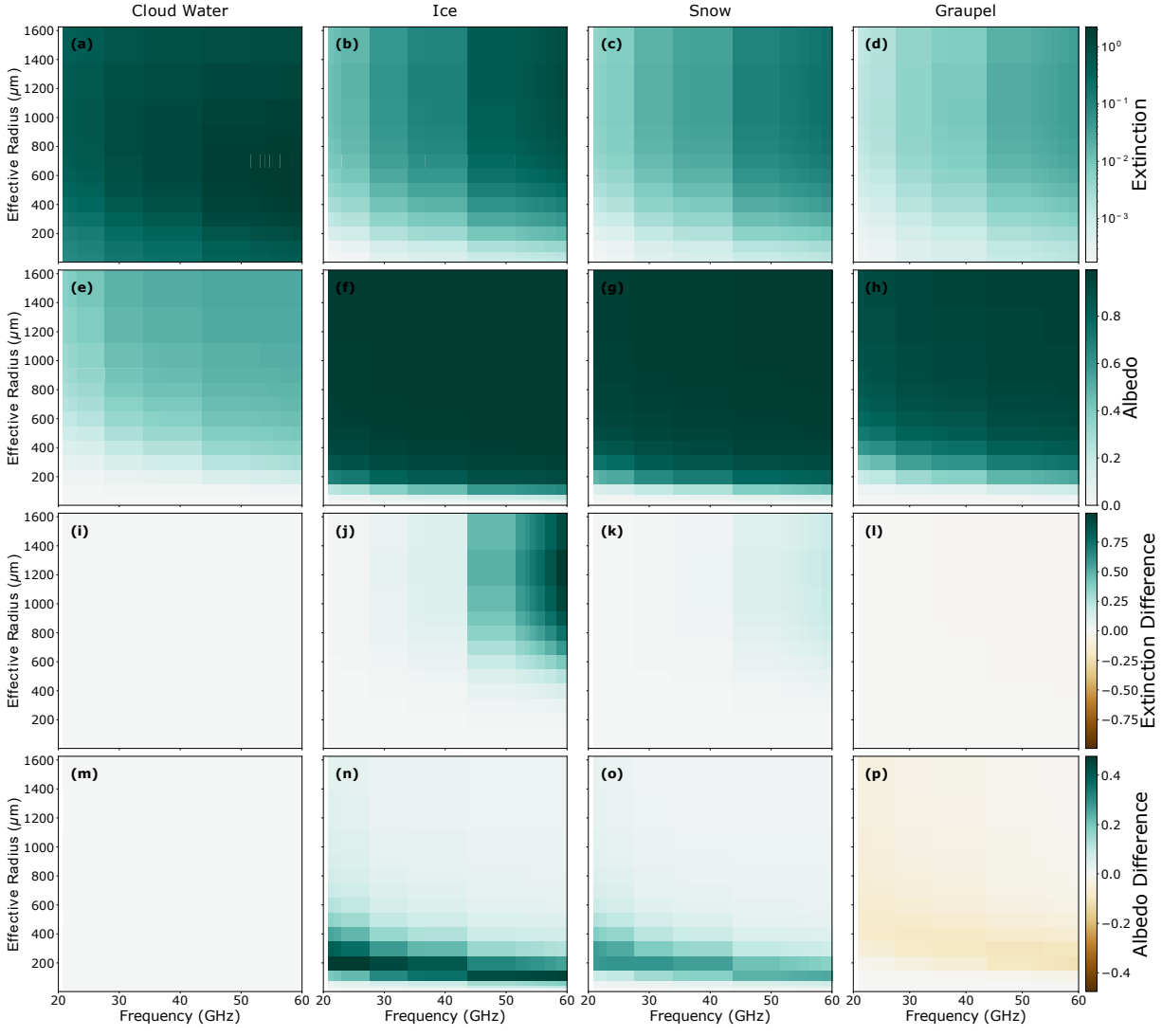

Figure 2: Scattering properties of the cloud particles. The top two rows (a-h) show the extinction coefficient and SSA of Mie, and the bottom two rows (i-p) show the corresponding difference between results computed from Mie and DDA.

https://doi.org/10.5194/egusphere-2025-5017
Preprint. Discussion started: 16 February 2026

2.2 Accelerated Discrete-Ordinate Adding Method

Ground-based microwave radiometers observe downwelling radiance primarily from atmospheric thermal emission, with the cosmic microwave background entering as the top boundary. Under clear-sky conditions, hydrometeors are absent and scattering is negligible, so the source function reduces to gaseous Planck emission with absorption, whereas in all-sky scenes, clouds and precipitation introduce extinction, emission, and multiple scattering. Accordingly, the monochromatic radiative transfer equation for a plane-parallel layer in the microwave band can be written as Eq. (1):

$$\mu \frac{dI(\tau,\mu,\phi)}{d\tau} = I(\tau,\mu,\phi) - (1-\omega)B(\tau) - \frac{\omega}{4\pi}\int_0^{2\pi} d\phi' \int_{-1}^{1} I\left(\tau,\mu',\phi'\right) P\left(\mu,\phi;\mu',\phi'\right) d\mu' \tag{1}$$

where $I(\tau,\mu,\phi)$ is the diffuse radiance along direction μ,ϕ at optical depth τ. The variable μ is the cosine of the viewing zenith angle and ϕ is the azimuth angle. $P\left(\mu,\phi;\mu',\phi'\right)$ and ω refer to the phase function, the SSA. $B(\tau)$ is the vertical distribution of the Planck function and we adopt the linear-in-tau approximation as:

$$B(\tau) = B_0(1+\beta\tau) \tag{2}$$

with

$$\beta = \left(B_1 / B_0 - 1\right) / \tau_0 \tag{3}$$

By expanding the phase function in a series of Legendre polynomials and the radiance $I(\tau,\mu,\phi)$ into a Fourier cosine series, the equation is replaced by $2M$ independent equations:

$$\mu \frac{dI^m(\tau,\mu)}{d\tau} = I^m(\tau,\mu) - \frac{\omega}{2}\int_{-1}^{1} I^m\left(\tau,\mu'\right) P^m\left(\mu,\mu'\right) d\mu' - \delta_{m,0}(1-\omega)B[T(\tau)] \tag{4}$$

with

$$I(\tau,\mu,\phi) = \sum_{m=0}^{2M-1} I^m(\tau,\mu)\cos\left[m\left(\phi-\phi_0\right)\right] \tag{5}$$

$$P^m\left(\mu,\mu'\right) = \sum_{l=m}^{2M-1} (2l+1)\bar{\omega}_l P_l^m(\mu) P_l^m\left(\mu'\right) \tag{6}$$

where $P_l^m(\mu)$ is associated Legendre polynomial, the expansion coefficient $\bar{\omega}_l$ can be determined from the orthogonal property of Legendre polynomials (Liou et al., 1988).

In radiative transfer simulations, the atmosphere is typically divided into multiple plane-parallel layers, which are categorized as either scattering or non-scattering. This study employs the an accelerated discrete ordinate method (ADOM, Shi et al., 2025b), where the Discrete Ordinates Method (DOM, Stamnes et al., 1988) is applied exclusively to the scattering layers. To enhance computational efficiency, adjacent non-scattering layers are merged based on non-scattering radiative transfer theory. Within the ADOM framework, the DOM is used to solve the radiative transfer equation for each scattering layer. By applying the discrete ordinates method, the integral form of Eq. (4) can be approximated as:

https://doi.org/10.5194/egusphere-2025-5017
Preprint. Discussion started: 16 February 2026

$$\int_{-1}^{1} I^m\left(\tau,\mu'\right)P^m\left(\mu,\mu'\right)d\mu' = \sum_{\substack{i=-N \\ i\neq 0}}^{N} a_i I^m\left(\tau,\mu_i\right)P^m\left(\mu,\mu_i\right) \tag{7}$$

where $2N$ is the number of streams, and N is typically set equal to M. The terms μ_i and a_i represent the Gaussian quadrature points and the corresponding weights, respectively. By substituting Eq. (7) into Eq. (4), the radiative transfer equation can be written in its discrete-ordinate form as:

$$\frac{d}{d\tau}\begin{bmatrix}\mathbf{i}_0^+\\ \mathbf{i}_0^-\end{bmatrix} = \begin{bmatrix}-\boldsymbol{\chi}_0 & -\boldsymbol{\gamma}_0\\ \boldsymbol{\gamma}_0 & \boldsymbol{\chi}_0\end{bmatrix}\begin{bmatrix}\mathbf{i}_0^+\\ \mathbf{i}_0^-\end{bmatrix} - \begin{bmatrix}\mathbf{q}_{\mathrm{ir}}\\ -\mathbf{q}_{\mathrm{ir}}\end{bmatrix}(1+\beta\tau), \tag{8}$$

with

$$\mathbf{i}_+^m(\tau) = \left[I^m\left(\tau,\mu_1\right) \quad \ldots \quad I^m\left(\tau,\mu_N\right)\right]^T \tag{9}$$

$$\mathbf{i}_-^m(\tau) = \left[I^m\left(\tau,\mu_{-1}\right) \quad \ldots \quad I^m\left(\tau,\mu_{-N}\right)\right]^T \tag{10}$$

The definitions of all symbols are consistent with those in Shi et al. Solving this equation yields the radiances at the top and bottom of the scattering layer.

In the non-scattering layer, the scattering term can be ignored in Eq. (4), and the solution for the downward radiation at the lower boundary of each layer is composed of two terms: (1) the downward radiation incident at the upper boundary, attenuated through the entire layer, and (2) the integrated, attenuated thermal emission from within the layer. The detailed derivations for both scattering and non-scattering layers are provided in Shi et al. After merging the non-scattering layers, ADOM yields a K-layer atmospheric profile. The upper boundary is set to the cosmic background radiation, while the lower boundary is determined by the surface thermal emission and diffuse reflection. To compute the radiance at an arbitrary viewing zenith angle, we introduce $\pm\mu_{\mathrm{sim}}$ as an additional Gaussian quadrature point with zero weight. The radiance at the specified viewing angle for a ground-based microwave radiometer can then be expressed as $I_K\left(\tau_K,-\mu_{\mathrm{sim}}\right)$.

3 Sensitivity of Microwave Brightness Temperatures to Hydrometeors

The interaction between microwave radiation and atmospheric hydrometeors plays a fundamental role in controlling the brightness temperatures observed by GMRs. Different hydrometeors influence radiative transfer through distinct physical mechanisms. Liquid water and rain primarily enhance absorption and emission, while ice and snow mainly affect the radiance field through scattering. As a result, the sensitivity of microwave radiances depends not only on the total hydrometeors content but also on their microphysical properties such as effective radius and phase. These sensitivities vary systematically across the microwave spectrum, leading to characteristic channel-dependent responses that offer crucial diagnostics for all-sky radiative transfer modeling.

https://doi.org/10.5194/egusphere-2025-5017
Preprint. Discussion started: 16 February 2026

Figure 3 shows the brightness-temperature responses of the YKW-1 radiometer at Yan'an to different hydrometeors, including cloud liquid water, rainwater, ice, and snow. The simulations were conducted under U.S. standard atmospheric conditions by introducing additional hydrometeors into representative layers: cloud liquid water and rainwater were perturbed in the lower troposphere (700–800 hPa), while ice and snow were perturbed in the mid-troposphere (366–545 hPa). For the water-content sensitivity tests, particles were prescribed with fixed effective radii (50 μm for cloud water and ice, 500 μm for rain and snow). For the effective-radius sensitivity tests, hydrometeor amounts were fixed (0.001 kg m^{-2} for cloud and rain, 0.01 kg m^{-2} for ice and snow) while particle sizes varied between 100 and 1000 μm. The brightness temperature response is quantified as the difference relative to clear-sky conditions ($\Delta BT = BT_{cloudy} - BT_{clear}$), thereby isolating the direct radiative contribution of each hydrometeor type. For liquid water particles, ΔBT is mainly positive because their dominant absorption and emission properties enhance the downwelling brightness temperature. This effect is most pronounced in the water-vapor absorption band (22–31 GHz) and the weak oxygen absorption band (52–54 GHz). The magnitude of the response increases nearly linearly with the liquid water path, while the particle effective radius modulates the balance between absorption and scattering. Smaller droplets perform almost entirely as absorbers, but larger particles cause significant scattering. Rainwater produces a similar, but stronger, spectral signature than cloud water, owing to the larger particle sizes and higher absorption efficiency of raindrops. In contrast, ice particles tend to produce negative ΔBT values because scattering dominates over absorption, causing radiation to deviate from the nadir direction and thereby reducing the observed brightness temperature. This reduction is particularly evident in the oxygen absorption band, where the atmosphere is already optically thick and additional scattering further amplifies the decrease. Compared with ice, snow has a slightly weaker impact on reducing brightness temperature due to its lower density.

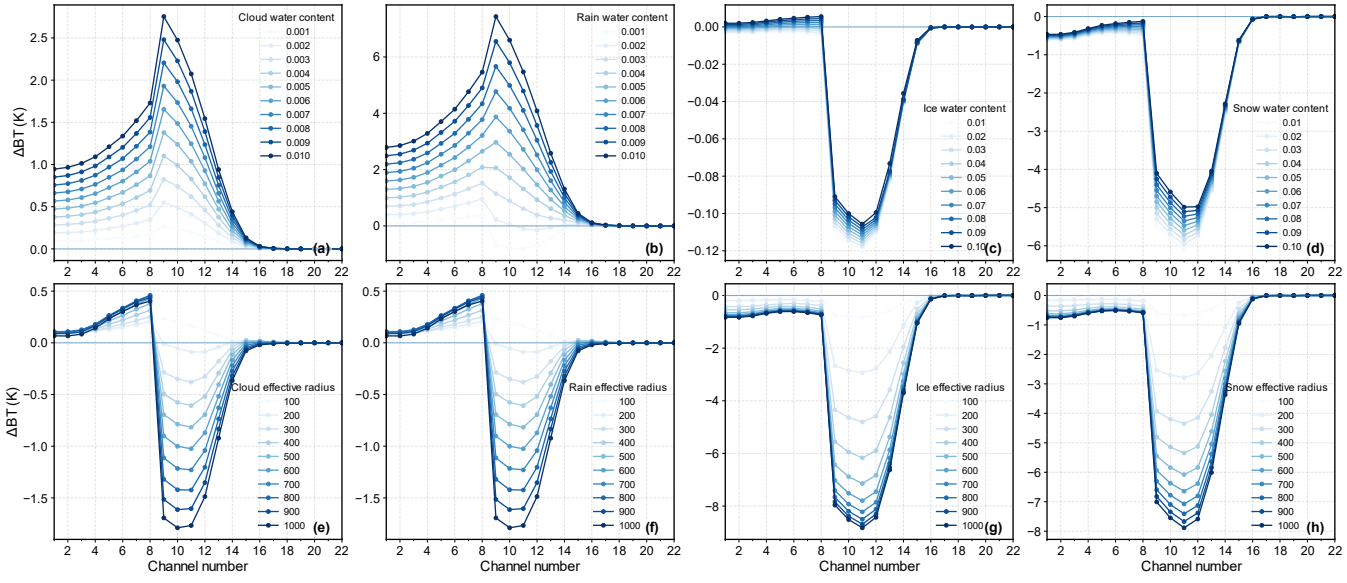

Figure 3: Clear-sky-referenced ΔBT for the YKW-1 at Yan'an in response to perturbations in hydrometeor content and effective radius, separated by cloud liquid water, rainwater, ice, and snow.

https://doi.org/10.5194/egusphere-2025-5017
Preprint. Discussion started: 16 February 2026

Jacobian analysis provides a complementary diagnostic of radiative transfer and is fundamental in retrieval and data assimilation because it links perturbations in atmospheric state variables to changes in observed brightness temperatures. In ARMS-gb v2.0, a complete tangent-linear model, adjoint model, and K-matrix mode are implemented to efficiently compute the Jacobians required for such applications. Figure 4 shows the mean Jacobians of cloud liquid water, rainwater, ice water, and snow water, based on six-month ERA5-driven simulations for YKW-1 at Yan'an under zenith viewing geometry. These Jacobians quantify how perturbations in hydrometeor content at different pressure levels alter the observed brightness temperatures, thereby providing a direct measure of vertical sensitivity. The brightness temperature of the GMR exhibits particular sensitivity to liquid water, with the strongest impact in the lower troposphere. Cloud liquid water shows pronounced sensitivity around 600 hPa, while rainwater peaks closer to the surface near 700 hPa. In contrast, the sensitivity to snow is much weaker than to liquid water, with limited absorption and emission producing only modest responses at altitudes of 5–9 km. Ice hydrometeors exhibit sensitivities an order of magnitude lower than snow, with Jacobians showing a slight bimodal structure. The Jacobians also show that the response peaks of different channels occur at nearly the same altitudes, differing mainly in magnitude, which indicates that ground-based microwave radiometers have limited vertical resolution in their sensitivity to hydrometeors.

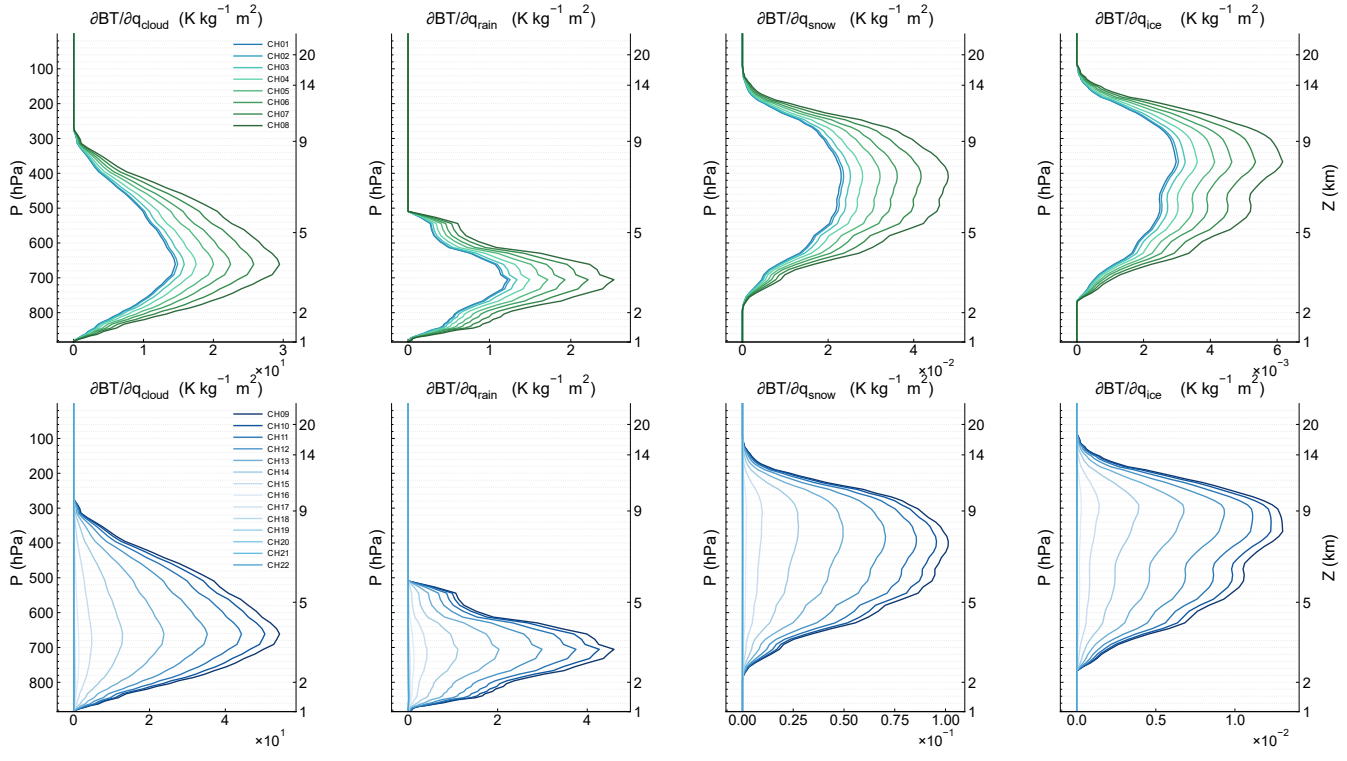

Figure 4: Jacobians of cloud liquid, cloud ice, rain, and snow water content, averaged over a six-month period and derived from radiative transfer (RT) simulations of the YKW-1 channel brightness temperatures at Yan'an station, driven by ERA5 data.

https://doi.org/10.5194/egusphere-2025-5017
Preprint. Discussion started: 16 February 2026

4 Evaluation in simulating real observations

To further evaluate the capability of ARMS-gb v2.0 for all-sky simulations, we conducted experiments driven by realistic atmospheric background profiles. The input profiles of temperature and humidity were taken from the hourly ERA5 reanalysis provided by ECMWF. In addition, vertical distributions of cloud liquid water, rainwater, ice water, and snow water contents were included to represent the cloud contributions, with the mixing ratios converted into layer-integrated water paths before input. Besides the YKW-1 at the Yan'an station mentioned above, we also simulated the YKW-2 located in Karamay (45.37°N, 84.51°E), using data from January to June 2025.

To analyze the contributions of individual hydrometeors under realistic atmospheric conditions, we used ERA5 profiles from the corresponding site for the period January–June 2025 as background input to perform simulations without hydrometeors as well as with each hydrometeor added separately. Figure 5 presents the mean differences obtained from these experiments. In the water-vapor absorption band between 22 and 31 GHz, liquid hydrometeors dominate the radiative impact. For YKW-2, cloud liquid water typically increases brightness temperatures by about 1–2 K, while rainwater produces stronger signals that exceed 2.5 K in channel 7. In terms of YKW-1, the effect is significantly greater, with cloud water biases exceeding 2 K and precipitation magnifying the deviations to roughly 3.5 K around channels 8–10. As the channel frequency increases, the impact of liquid water vapor on brightness temperature gradually decreases after reaching the oxygen absorption band. As the frequency approaches the weak oxygen absorption band (51–55 GHz), the scattering effect of frozen water particles on the signal becomes most significant. The temperature drop caused by small ice crystals is approximately -0.2 K, while the temperature drop caused by snowflakes is much larger, reaching around -1.5 K. At frequencies above 55 GHz, especially near the center of the oxygen absorption line, the atmosphere's absorption of electromagnetic waves becomes very strong; at this point, the emitted radiation is primarily determined by the absorption of molecular oxygen. Therefore, the error caused by cloud particles becomes negligible. When considering the combined effects of all hydrometeor species, YKW-1 and YKW-2 show nearly consistent behavior. The brightness temperature increases with frequency across the water-vapor absorption band and reaches a maximum near its upper end. As the frequency increases, the impact gradually weakens but remains noticeable in the weak oxygen absorption band. In the YKW-1 simulation, hydrometeors cause a warming of nearly 3 K at channel 7. For YKW-2, the overall change in brightness temperature is smaller than for YKW-1, and at channels 9 and 10, liquid water even exhibits scattering dominance, leading to a reduction in brightness temperature. This frequency-dependent pattern suggests that the radiative effects of liquid and frozen hydrometeors interact within the two major absorption bands, underscoring the importance of properly accounting for hydrometeors in applications.

https://doi.org/10.5194/egusphere-2025-5017
Preprint. Discussion started: 16 February 2026

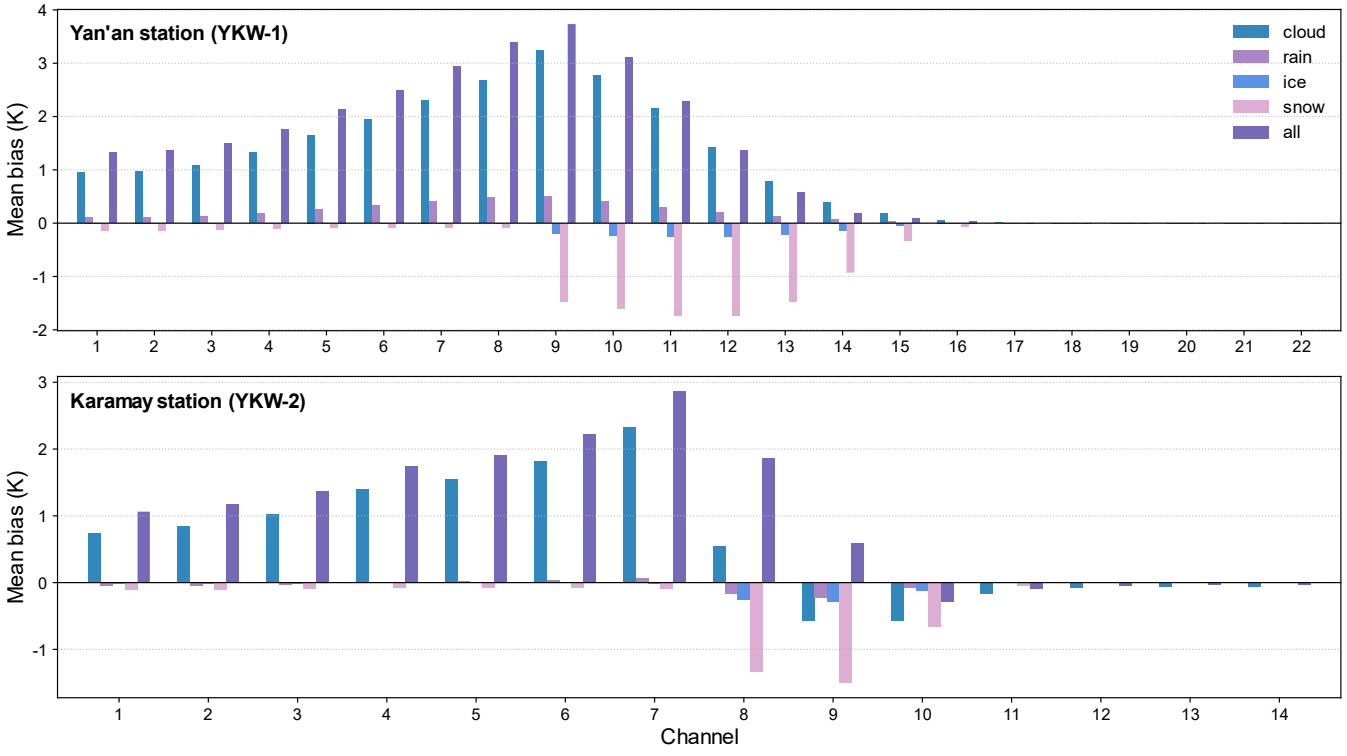

Figure 5: Mean differences in simulated brightness temperatures (simulation with cloud effects minus simulation without) for the (a) YKW-1 at Yan'an station and (b) YKW-2 at Karamay station. The colors distinguish the contributions from various hydrometeors and their combined effect.

Comparing simulations with observations under all-sky conditions provides a direct assessment of a radiative transfer model's performance. We evaluated the performance of ARMS-gb v2.0 under cloudy, non-precipitating conditions from April to June 2025 at two sites, YKW-1 in Yan'an and YKW-2 in Karamay, testing LUTs based on Mie and DDA. For reference, we also compared with ARMS-gb v1.0, which neglects cloud water, and we ran RTTOV-gb on identical background fields; RTTOV-gb includes absorption and emission by cloud liquid water. Mean O-B results for each channel are shown in Fig. 6. It is important to note that the calibration quality at YKW-1 and YKW-2 is not consistently stable, and clear-sky O-B are occasionally large, which poses challenges for the all-sky simulations. Cloudy-sky O-B values that approach the clear-sky O-B indicate more accurate cloud representation. For clarity, the clear-sky simulation errors are shown as gray bars. Compared with ARMS-gb v1.0, both ARMS-gb v2.0 lookup-table schemes bring O-B significantly closer to the clear-sky baseline across the water-vapor band and the weak oxygen band, reflecting an effective representation of hydrometeor absorption and scattering. The Mie and DDA LUTs perform similarly overall, with DDA slightly outperforming in several channels. In the oxygen absorption channels that are insensitive to hydrometeors, all models produce O-B values close to the clear-sky errors. For YKW-1, the clear-sky bias is relatively large, with local maxima of about 5 K near channels 5 and 10. ARMS-gb v1.0 shows even larger O-B values, with deviations of nearly 4 K from the clear-sky reference at channel 5 and about 2 K across channels 6–12. In contrast, both all-sky schemes significantly improve the results, generally keeping O-B within ±1 K of the

https://doi.org/10.5194/egusphere-2025-5017
Preprint. Discussion started: 16 February 2026

clear-sky baseline. For YKW-2, the clear-sky error in the water-vapor channels (1–6) remains around 0.5 K, but a pronounced systematic bias of about 3 K appears at channel 7 and gradually decreases to about 1 K at higher frequencies. ARMS-gb v1.0 produces biases of 1–2 K in the water-vapor band, exceeding 2 K in channels 7–9. In contrast, ARMS-gb v2.0 provides
290 significant improvements, with O-B values fluctuating within ±1 K of the clear-sky reference. RTTOV-gb exhibits small improvements relative to ARMS-gb v1.0 under cloudy conditions, mainly across channels 4–12 at YKW-1 and 4–9 at YKW-2, owing to its inclusion of liquid-cloud absorption. ARMS-gb performs better in humid environments due to the inclusion of 2-m humidity and an improved gas-absorption scheme (Shi et al., 2025a), while RTTOV-gb produces larger errors than ARMS-gb v1.0 in channels 1–3 for YKW-1 and 1–2 for YKW-2, as well as in channels 14–15 for YKW-1 and channel 10 for
295 YKW-2.

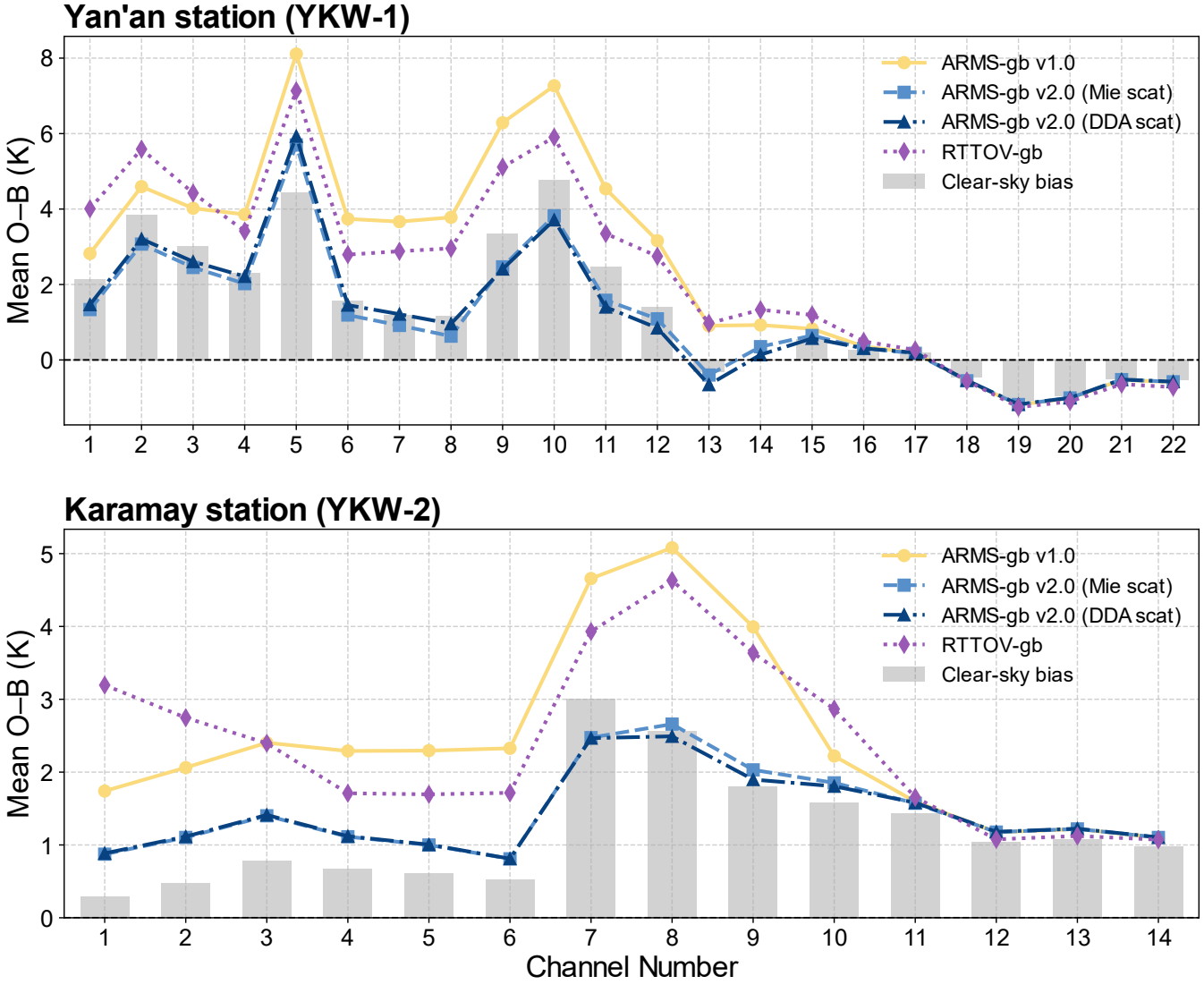

https://doi.org/10.5194/egusphere-2025-5017
Preprint. Discussion started: 16 February 2026

Figure 6: Mean O-B biases for the Yan'an station (YKW-1) and Karamay station (YKW-2) radiometers during April–June 2025. The comparison includes simulations from ARMS-gb v1.0, ARMS-gb v2.0 using Mie and DDA scattering, and RTTOV-gb. The gray bars indicate the mean O-B for clear-sky conditions over the same period.

Given the high temporal resolution of ground-based microwave radiometers, the ability of the model to reproduce instantaneous brightness temperature maxima is of particular importance. To demonstrate the capability of the all-sky model in simulating brightness temperature maxima, we compared observations with all-sky simulations for the period from April to June 2025. Rainy periods were identified using the radiometer's built-in precipitation sensor and are indicated by shaded areas in Fig. 7. For consistency, the frequency bands shown are the same as those in Fig. 1. The agreement between observations and simulations under cloudy but non-rainy conditions improves substantially when cloud effects are included in the model. In both the water-vapor and oxygen absorption bands, the all-sky model successfully reproduces the observed peaks and the sustained enhancement associated with increased cloud liquid water, although the accuracy still depends on the background fields and the cloud water profiles. Nevertheless, Fig. 7 demonstrates that the model captures the essential absorption and emission processes of water vapor. In contrast, during rainfall events, notable discrepancies occur: the model occasionally fails to reproduce the observed maxima and tends to underestimate the brightness temperature. The temperature-sensitive channels, being less affected by water vapor, show relatively better performance under rainy conditions.

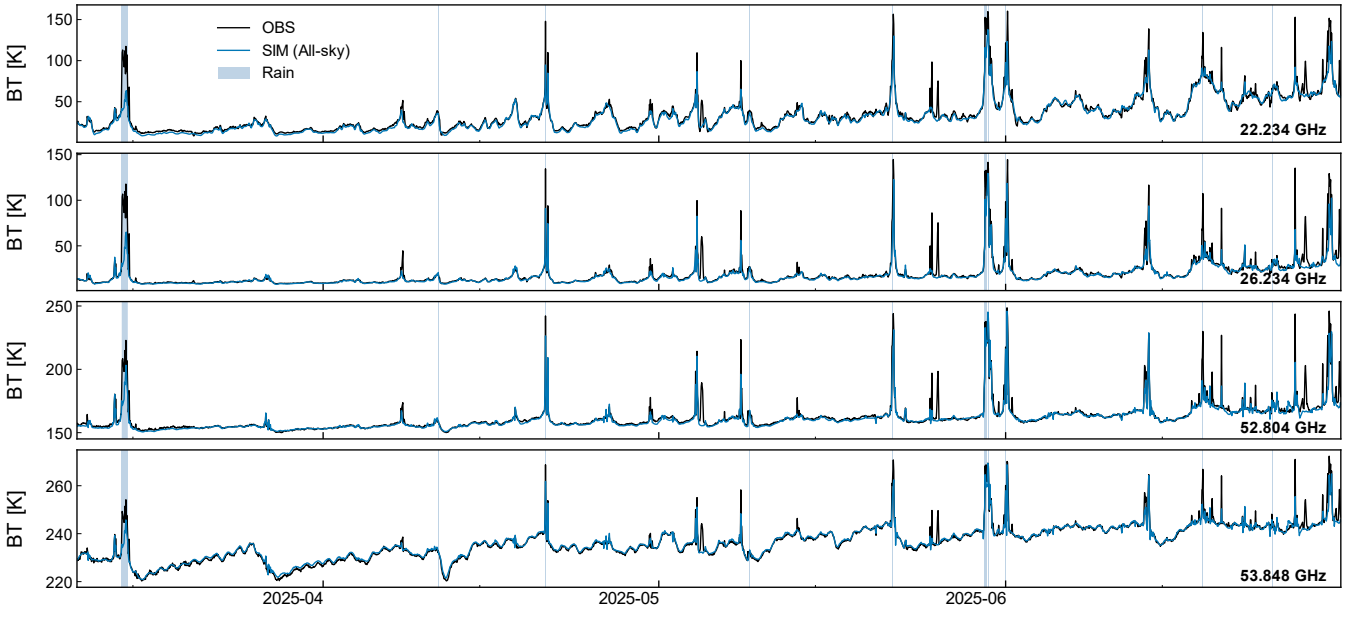

Figure 7: Six-month time series comparison of observed brightness temperatures (black) with all-sky simulations (blue) for representative channels of the Yan'an station radiometers. Shaded areas indicate periods with precipitation.

To evaluate model performance, we compiled statistics for simulations from ARMS-gb v1.0, RTTOV-gb, and ARMS-gb v2.0 at Yan'an station under cloudy-no-rain conditions during January–June 2025, based on 2,136 cases. Figure 8 shows OBS–SIM scatterplots with regression lines, together with correlation coefficient (R^2), root mean square error (RMSE), and median O-B; probability density functions (PDFs) for the observations and for each model are displayed above each panel. Generally,

https://doi.org/10.5194/egusphere-2025-5017
Preprint. Discussion started: 16 February 2026

ARMS-gb v2.0 provides the closest agreement. At 22.234 GHz, R^2 rises from 0.89 for ARMS-gb v1.0 to 0.95 for ARMS-gb v2.0, and the model and observed PDFs align closely, while RTTOV-gb performs between the two. Errors increase with frequency within the vapor band and reach a maximum at 30.000 GHz, where ARMS-gb v2.0 attains 0.71 of R^2, compared with 0.34 for ARMS-gb v1.0. In the weak oxygen absorption band at 51.248 GHz, ARMS-gb v1.0 exhibits large discrepancies, with RMSE = 8.57 K and low correlation, whereas ARMS-gb v2.0 reduces the RMSE to 4.02 K and increases the correlation to R^2 = 0.85; RTTOV-gb shows partial improvement but remains below ARMS-gb v2.0. At the higher-frequency oxygen channels near 53–55 GHz, all three models track the observations closely and approach the 1:1 line, although ARMS-gb v2.0 generally retains the lowest RMSE and the tightest scatter. Overall, the statistics and PDFs in Fig. 8 indicate that the all-sky model reduces systematic bias and improves correlation relative to both ARMS-gb v1.0 and RTTOV-gb, with the largest gains in the water-vapor band and the mid-frequency oxygen channel where hydrometeor effects are strongest.

https://doi.org/10.5194/egusphere-2025-5017
Preprint. Discussion started: 16 February 2026

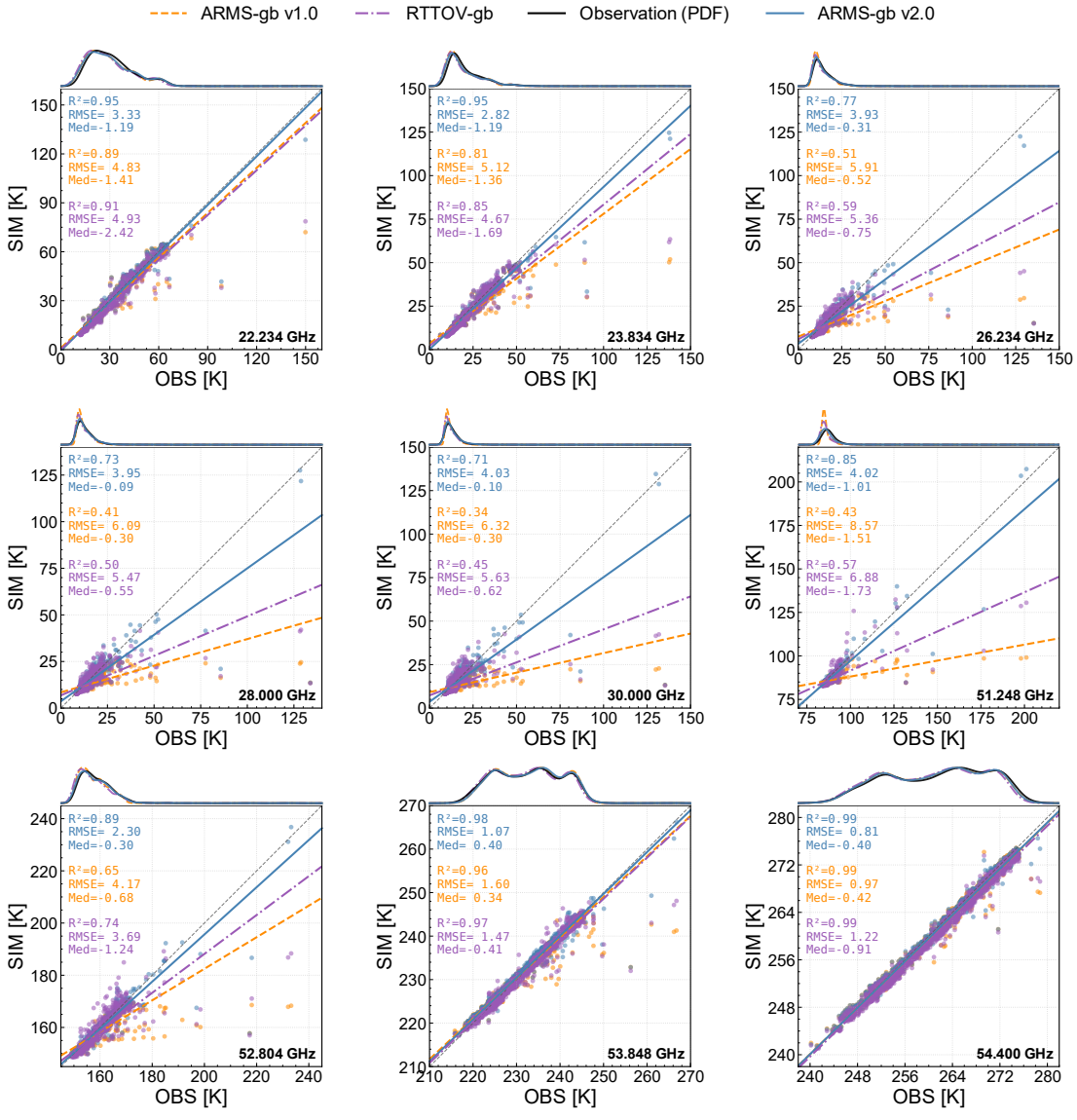

Figure 8: Scatter plots of observed versus simulated brightness temperatures at selected YKW-1 channels, comparing ARMS-gb v1.0, v2.0, and RTTOV-gb with regression lines and summary statistics. Marginal PDFs of observations (black) and simulations are shown above each panel.

Accurate characterization of the error covariance of the observation operator is a key requirement for data assimilation and atmospheric retrieval applications. Since processes such as the growth and decay of the atmospheric boundary layer and the formation and evolution of clouds exhibit pronounced diurnal cycles, model simulation errors may also display systematic diurnal variations. Figure 9 shows the diurnal cycle of O-B biases for a YKW-1 radiometer site during January–June 2025 (local time). Distinct diurnal patterns are evident across both water-vapor band and oxygen band channels. In the low-frequency water-vapor channels (channels 1–7), biases are weakly positive overnight and peak in the early morning hours (+1–3 K),

https://doi.org/10.5194/egusphere-2025-5017
Preprint. Discussion started: 16 February 2026

decrease to near-zero or slightly negative values around midday (−1 to −2 K), and rise again in the late afternoon and evening. In the oxygen absorption band (channel 8–14), systematic variations are more distinct: channels 9–12 exhibit strong negative biases around midday (−3 to −6 K) and positive maxima in the evening (+3 to +6 K), with a secondary positive peak also emerging in the early morning. At higher frequencies (channel 15–22), the diurnal variations are much smaller, remaining close to zero throughout the day. These features reflect a combination of atmospheric and instrumental factors. On the atmospheric side, mismatches between model and boundary-layer evolution can lead to midday cold biases in oxygen-band channels and early morning humidity-related biases in vapor channels. On the instrumental side, calibration drifts and thermal effects also play an important role. Cooler nighttime conditions reduce receiver gain and suppress measured brightness temperatures, while daytime heating increases noise temperature and produces higher values. Together, these processes generate the characteristic transition from negative midday biases to positive evening values. The results highlight the need to account for diurnal error structures when applying all-sky simulations in retrieval and assimilation systems.

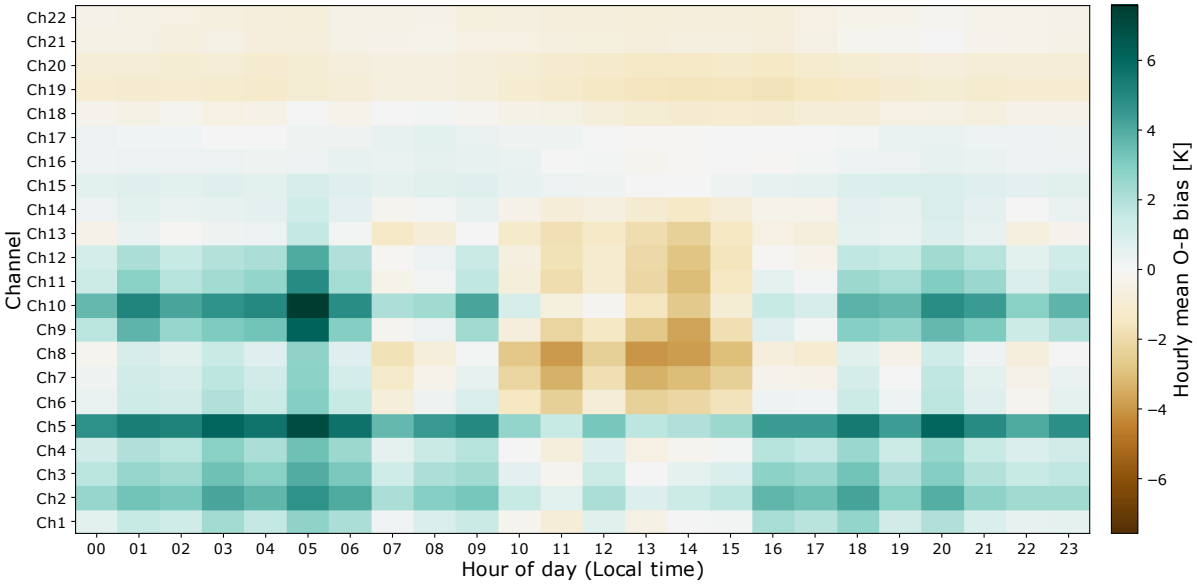

Figure 9: Diurnal variation of the mean O-B bias Yan'an station (YKW-1) from January to June 2025. The time is shown in local time (UTC+8).

A core prerequisite for effectively applying all-sky ground-based microwave radiometer observations to numerical weather prediction and nowcasting is not only the accurate simulation of brightness temperatures under all weather conditions, but also the quantitative estimation of their observational errors. This requirement is particularly critical during rainfall, which remains one of the most challenging scenarios. Rainfall is not only a key source and sink of atmospheric heat and moisture but also introduces substantial complexity into radiative transfer due to its strong and variable electromagnetic scattering properties, thereby increasing both the difficulty and the uncertainty of simulations. Figure 10 shows the mean O-B bias and RMSE for the YKW-1, collected from all hourly data between January and June 2025 and stratified into clear-sky, cloudy, and precipitation conditions. It is evident that under clear-sky conditions, ARMS-gb exhibits the smallest errors, with mean O-B

https://doi.org/10.5194/egusphere-2025-5017
Preprint. Discussion started: 16 February 2026

generally within 1 K and RMSE around 2 K. Under cloudy, non-precipitating conditions, both the mean bias and RMSE increase slightly, while RMSE remains below 3 K for most channels. However, in rainy conditions, errors rise sharply, with RMSE exceeding 35 K in the water-vapor band and peaking above 40 K at channel 7, while the mean O-B shows a substantial positive bias of nearly 30 K. In cloudy and precipitating conditions, water-vapor and weak-oxygen channels exhibit larger errors than temperature channels, while their sensitivity to cloud and rain particles progressively diminishes with increasing frequency. Notably, channel 3 shows an overall negative mean O-B under clear-sky and cloudy conditions, and a markedly smaller mean O-B than adjacent channels during precipitation, which is attributable to instrument calibration issues. These errors mainly arise from two sources: the uncertainties in cloud water profiles and the strong sensitivity of the instrument to environmental influences. Under precipitation conditions, raindrops exhibit complex and highly variable size distributions during formation and fall, which introduces additional uncertainties in absorption and scattering and thus requires specific parameterization. At the same time, raindrops accumulating on the radome modify its transmittance and refractive index, effectively acting as an extra absorbing layer that elevates the measured brightness temperatures. In addition, raindrop impacts and the evaporation of surface water near the instrument may further perturb the near-surface microwave environment. The combined effects of atmospheric processes and instrument-related factors lead to the pronounced errors observed during rainy conditions, underscoring the need for comprehensive characterization of both physical scattering processes and instrument uncertainties when applying ground-based microwave radiometers in assimilation and retrieval systems.

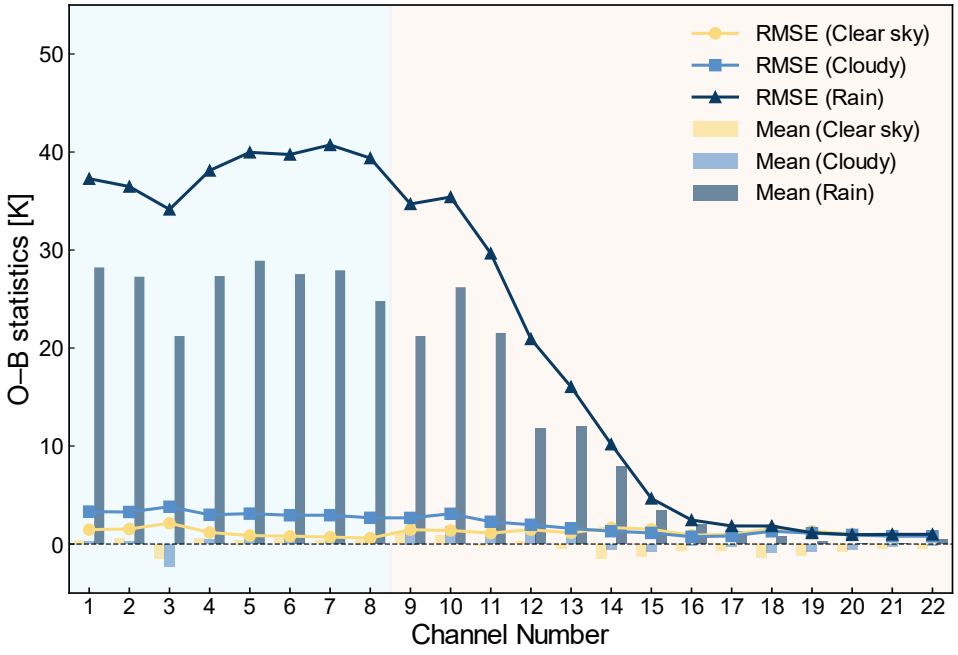

Figure 10: RMSE and mean O-B for the YKW-1 at Yan'an station across all channels during January and June 2025, grouped by clear-sky, cloudy, and rainy conditions.

https://doi.org/10.5194/egusphere-2025-5017
Preprint. Discussion started: 16 February 2026

5 Conclusions

This study developed ARMS-gb v2.0, a fast all-sky radiative transfer model for ground-based microwave radiometers. The model extends the previous version by adding a cloud-particle absorption and scattering module, implementing a discrete-ordinate adding method for multiple scattering, and provides tangent-linear and adjoint capabilities for all-sky variational applications. It supports simulations of cloud water, rain, ice, snow, and graupel using optical-property LUTs computed with Mie theory for liquid hydrometeors and DDA for frozen hydrometeors. Sensitivity experiments demonstrate that liquid species increase brightness temperatures through absorption and emission, whereas frozen species decrease them through scattering.

To validate ARMS-gb v2.0 under all-sky conditions, we conducted six-month experiments with the 14-channel GMRs and 22-channel GMRs deployed in China. The model reproduces all-sky brightness temperatures well, and under cloudy conditions the mean O-B across channels remains within ~1 K. Relative to a model that neglects cloud effects, accuracy improves markedly, with RMSE dropping by 1–2 K in strong water-vapor channels, the 30 GHz correlation increasing from 0.34 to 0.71, O-B decreasing by 3–4 K in the weak oxygen band, and the 51.248 GHz correlation rising from 0.43 to 0.85. Generally, DDA and Mie perform similarly, but DDA more often aligns with the clear-sky bias in most channels. Nonetheless, precipitation remains the principal limitation, with large simulation errors in rainy conditions. As a result, assimilation and retrieval in rainy conditions still require enhanced observation-error modeling, channel-dependent quality control, and cross-frequency consistency checks. Future work will extend instrument coverage, including higher-frequency systems, better characterize rainfall-related uncertainties, and couple ARMS-gb v2.0 with one-dimensional variational retrievals and operational data-assimilation systems to fully exploit boundary-layer information under truly all-sky conditions.

Code and data availability. Codes of ARMS-gb v2.0 are available at https://doi.org/10.5281/zenodo.17318669 (Huang et al., 2025). The 137-level ERA5 reanalysis data are available from the Copernicus Climate Data Store at https://doi.org/10.24381/cds.143582cf (Hersbach et al., 2017). Observations from GMRs at Karamay and Yan'an used in this study can be obtained from China Meteorological Administration Data As A Service (CMADaaS) under an available license (https://data.cma.cn/en, China Meteorological Administration, 2025). RTTOV-gb can be downloaded from the EUMETSAT NWP SAF website https://nwp-saf.eumetsat.int/site/software/rttov-gb/ (De Angelis et al., 2016; Cimini et al., 2019).

Author contributions. ZH and YS developed the model code and prepared the initial draft. JY and FW offered the conception of the study and led the model development. All authors discussed this work and reviewed the paper.

Competing interests. The authors declare that they have no conflict of interest.

https://doi.org/10.5194/egusphere-2025-5017
Preprint. Discussion started: 16 February 2026

Financial support. This research was funded by the National Natural Science Foundation of China (grant nos. U2542214, U2142212 and 42305162), the National Key Research and Development Program of China (grant no. 2021YFB3900400), and the Hunan Provincial Natural Science Foundation of China (grant no. 2021JC0009).

References

Bauer, P., Geer, A. J., Lopez, P., and Salmond, D.: Direct 4D-Var assimilation of all-sky radiances. Part I: Implementation, Q. J. R. Meteorolog. Soc., 136, 1868–1885, 2010.

Cao, Y., Shi, B., Zhao, X., Yang, T., and Min, J.: Direct Assimilation of Ground-Based Microwave Radiometer Clear-Sky Radiance Data and Its Impact on the Forecast of Heavy Rainfall, Remote Sensing, 15, 4314, https://doi.org/10.3390/rs15174314, 2023.

Cimini, D., Hewison, T. J., Martin, L., Güldner, J., Gaffard, C., and Marzano, F. S.: Temperature and humidity profile retrievals from ground-based microwave radiometers during TUC, metz, 15, 45–56, https://doi.org/10.1127/0941-2948/2006/0099, 2006.

Cimini, D., Hocking, J., De Angelis, F., Cersosimo, A., Di Paola, F., Gallucci, D., Gentile, S., Geraldi, E., Larosa, S., Nilo, S., Romano, F., Ricciardelli, E., Ripepi, E., Viggiano, M., Luini, L., Riva, C., Marzano, F. S., Martinet, P., Song, Y. Y., Ahn, M. H., and Rosenkranz, P. W.: RTTOV-gb v1.0 – updates on sensors, absorption models, uncertainty, and availability, Geosci. Model Dev., 12, 1833–1845, https://doi.org/10.5194/gmd-12-1833-2019, 2019.

Clough, S. A., Shephard, M. W., Mlawer, E. J., Delamere, J. S., Iacono, M. J., Cady-Pereira, K., Boukabara, S., and Brown, P. D.: Atmospheric radiative transfer modeling: a summary of the AER codes, Journal of Quantitative Spectroscopy and Radiative Transfer, 91, 233–244, https://doi.org/10.1016/j.jqsrt.2004.05.058, 2005.

Council, N. R., Studies, D. on E. and L., Climate, B. on A. S. and, and Needs, C. on D. M. M. O. C. to M. M. N.: Observing Weather and Climate from the Ground Up: A Nationwide Network of Networks, National Academies Press, 250 pp., 2009.

De Angelis, F., Cimini, D., Löhnert, U., Caumont, O., Haefele, A., Pospichal, B., Martinet, P., Navas-Guzmán, F., Klein-Baltink, H., Dupont, J.-C., and Hocking, J.: Long-term observations minus background monitoring of ground-based brightness temperatures from a microwave radiometer network, Atmos. Meas. Tech., 10, 3947–3961, https://doi.org/10.5194/amt-10-3947-2017, 2017.

Draine, B. T. and Flatau, P. J.: Discrete-Dipole Approximation For Scattering Calculations, J. Opt. Soc. Amer. A, 11, 1491, https://doi.org/10.1364/JOSAA.11.001491, 1994.

Garnett, J. M.: VII. Colours in metal glasses, in metallic films, and in metallic solutions.—II, Philosophical Transactions of the Royal Society of London. Series A, Containing Papers of a Mathematical or Physical Character, 205, 237–288, 1906.

Geer, A. J., Baordo, F., Bormann, N., Chambon, P., English, S. J., Kazumori, M., Lawrence, H., Lean, P., Lonitz, K., and Lupu, C.: The growing impact of satellite observations sensitive to humidity, cloud and precipitation: Impact of Satellite Humidity, Cloud and Precipitation Observations, Q. J. R. Meteorolog. Soc., 143, 3189–3206, https://doi.org/10.1002/qj.3172, 2017.

Hersbach, H., Bell, B., Berrisford, P., Hirahara, S., Horányi, A., Muñoz-Sabater, J., Nicolas, J., Peubey, C., Radu, R., and Schepers, D.: The ERA5 global reanalysis, Q. J. R. Meteorolog. Soc., 146, 1999–2049, 2020.

https://doi.org/10.5194/egusphere-2025-5017
Preprint. Discussion started: 16 February 2026

Hu, H. and Han, Y.: Comparing the Thermal Structures of Tropical Cyclones Derived From Suomi NPP ATMS and FY-3D Microwave Sounders, IEEE Trans. Geosci. Remote Sensing, 59, 8073–8083, https://doi.org/10.1109/TGRS.2020.3034262, 2021.

Huang, Z., Lu, H., Ma, Z., Shi, Y., Han, Y., Hu, H., and Yang, J.: A Nonspherical Cloud Scattering Database Using Aggregates of Roughened Bullet Rosettes Model for the Advanced Radiative Transfer Modeling System (ARMS), Adv. Atmos. Sci., 42, 1483–1498, https://doi.org/10.1007/s00376-024-4117-7, 2025.

Liou, K.-N., Fu, Q., and Ackerman, T. P.: A Simple Formulation of the Delta-Four-Stream Approximation for Radiative Transfer Parameterizations, Journal of Atmospheric Sciences, 45, 1940–1948, https://doi.org/10.1175/1520-0469(1988)045%253C1940:ASFOTD%253E2.0.CO;2, 1988.

Madhulatha, A., Rajeevan, M., Venkat Ratnam, M., Bhate, J., and Naidu, C. V.: Nowcasting severe convective activity over southeast India using ground-based microwave radiometer observations, JGR Atmospheres, 118, 1–13, https://doi.org/10.1029/2012JD018174, 2013.

Martinet, P., Cimini, D., Burnet, F., Ménétrier, B., Michel, Y., and Unger, V.: Improvement of numerical weather prediction model analysis during fog conditions through the assimilation of ground-based microwave radiometer observations: a 1D-Var study, Atmos. Meas. Tech., 13, 6593–6611, https://doi.org/10.5194/amt-13-6593-2020, 2020.

Mätzler, C. (Ed.): Thermal Microwave Radiation: Applications for Remote Sensing, Institution of Engineering and Technology, https://doi.org/10.1049/PBEW052E, 2006.

Ray, P. S.: Broadband complex refractive indices of ice and water, Applied optics, 11, 1836–1844, 1972.

Rosenkranz, P. W.: Water vapor microwave continuum absorption: A comparison of measurements and models, Radio Science, 33, 919–928, https://doi.org/10.1029/98RS01182, 1998.

Saunders, R., Matricardi, M., and Brunel, P.: An improved fast radiative transfer model for assimilation of satellite radiance observations: ASSIMILATION OF SATELLITE RADIANCE OBSERVATIONS, Q. J. R. Meteorolog. Soc., 125, 1407–1425, https://doi.org/10.1002/qj.1999.49712555615, 1999.

Shi, Y.-N., Yang, J., Han, W., Han, L., Mao, J., Kan, W., and Weng, F.: Development of a fast radiative transfer model for ground-based microwave radiometers (ARMS-gb v1.0): validation and comparison to RTTOV-gb, Geosci. Model Dev., 18, 1947–1964, https://doi.org/10.5194/gmd-18-1947-2025, 2025a.

Shi, Y.-N. and Weng, F.: An accelerated discrete ordinate method (ADOM) developed for scalar radiative transfer by merging adjacent clear-sky atmospheric layers: Forward and Jacobians derivation. Journal of Advances in Modeling Earth Systems, 17, e2025MS005136, 2025b

Stamnes, K., Tsay, S.-C., Wiscombe, W., and Jayaweera, K.: Numerically stable algorithm for discrete-ordinate-method radiative transfer in multiple scattering and emitting layered media, Appl. Opt., 27, 2502, https://doi.org/10.1364/AO.27.002502, 1988.

Wei, Y., Peng, K., Ma, Y., Sun, Y., Zhao, D., Ren, X., Yang, S., Ahmad, M., Pan, X., Wang, Z., and Xin, J.: Validation of ERA5 Boundary Layer Meteorological Variables by Remote-Sensing Measurements in the Southeast China Mountains, Remote Sensing, 16, 548, https://doi.org/10.3390/rs16030548, 2024.

https://doi.org/10.5194/egusphere-2025-5017
Preprint. Discussion started: 16 February 2026

Weng, F. and Liu, Q.: Satellite Data Assimilation in Numerical Weather Prediction Models. Part I: Forward Radiative Transfer and Jacobian Modeling in Cloudy Atmospheres, J. Atmospheric Sci., 60, 2633–2646, https://doi.org/10.1175/1520-0469(2003)060%253C2633:SDAINW%253E2.0.CO;2, 2003.

Weng, F., Han, Y., van Delst, P., Liu, Q., Kleespies, T., Yan, B., and Marshall, J. L.: JCSDA Community Radiative Transfer Model (CRTM), in: Proceeding of 14th International ATOVS Study Conference, Beijing, China, 2005.

Weng, F., Yu, X., Duan, Y., Yang, J., and Wang, J.: Advanced Radiative Transfer Modeling System (ARMS): A New-Generation Satellite Observation Operator Developed for Numerical Weather Prediction and Remote Sensing Applications, Adv. Atmos. Sci., 37, 131–136, https://doi.org/10.1007/s00376-019-9170-2, 2020.

Wu, J., Guo, J., Yun, Y., Yang, R., Guo, X., Meng, D., Sun, Y., Zhang, Z., Xu, H., and Chen, T.: Can ERA5 reanalysis data characterize the pre-storm environment?, Atmospheric Research, 297, 107108, https://doi.org/10.1016/j.atmosres.2023.107108, 2024.

Yang, J. and Min, Q.: A passive and active microwave-vector radiative transfer (PAM-VRT) model, J. Quant. Spectrosc. Radiat. Transfer, 165, 123–133, https://doi.org/10.1016/j.jqsrt.2015.06.028, 2015.

Yang, J., Ding, S., Dong, P., Bi, L., and Yi, B.: Advanced radiative transfer modeling system developed for satellite data assimilation and remote sensing applications, J. Quant. Spectrosc. Radiat. Transfer, 251, 107043, https://doi.org/10.1016/j.jqsrt.2020.107043, 2020.